# The Adriatic Thrust Fault of the 2021 Seismic Sequence Estimated from Accurate Earthquake Locations Using *sP* Depth Phases

Raffaele Di Stefano*[1], Maria Grazia Ciaccio[1], Paola Baccheschi[1], and Dapeng Zhao[2]

## ABSTRACT

**An earthquake sequence occurred in the Central Adriatic region during March–June 2021. This sequence started on 27 March with a mainshock of moment magnitude ($M_w$) 5.2 occurring at 13:47 coordinated universal time (UTC). No foreshock was observed before this mainshock. The sequence lasted approximately three months, until the end of June 2021. Approximately 200 seismic events were recorded by the regional seismic network during this time, including four M ≥ 4.0 earthquakes. The 27 March 2021 earthquake was one of the strongest instrumentally recorded events in the area bounded approximately by the Ancona–Zadar line to the north and the Gargano–Dubrovnik line to the south. The mainshock originated at a focal depth of 9.9 km. The seismicity spread from the mainshock up-dip and down-dip along a northeast-dipping plane. Here, we investigate the geometry of the fault activated by this seismic sequence by using *sP* depth phases. We aim to significantly reduce the large uncertainties associated with the hypocentral locations of offshore earthquakes beneath the Adriatic Sea—an area that plays a fundamental role in the geodynamics of the Mediterranean. These refined earthquake locations also allow us to make inferences with regards to the seismotectonic context responsible for the analyzed seismicity, thus identifying a structure (here referred to as the Mid-Adriatic fault) consisting of a northwest–southeast-striking thrust fault with a ∼35° northeast-dipping plane. The use of depth-phase arrival times to constrain off-network event locations is of particular interest in Italy due to both the peculiar shape of the peninsula and the extreme scarcity of seafloor stations, the cost and management of which are very expensive and complex. Here, we present the first attempt to apply this off-network locating technique to the Italian offshore seismicity research with the aim of improving hazard estimations in these hard-to-monitor regions.**

## KEY POINTS

- We study the location of 70 M ≥ 2.9 earthquakes of the 2021 seismic sequence offshore Italy–Croatia.
- *sP* converted phases provide strong constraints on the focal depths of off-network earthquakes.
- The precise fault geometry has important implications for seismotectonics in the Adriatic.

**Supplemental Material**

## INTRODUCTION

The Adriatic microplate (D'Agostino *et al.*, 2008), hosting the Adriatic Sea, is located between the European and African major plates, and has played a major role in the tectonic history of the central Mediterranean region (Fig. 1). Many researchers assume that Adria moved as a single block, whereas other researchers, based on seismic and geodetic investigations, suggest that the microplate may have fragmented into two blocks that are currently rotating with respect to each other (Le Breton *et al.*, 2017, and references therein). Indeed, seismic reflection profiles—Global Positioning System-derived velocities and diffuse seismicity in the central area have been interpreted as evidence for the fragmentation of the Adriatic plate, suggesting that the northern part rotates independently and in opposite direction (counter clockwise) from the southern part

1. Istituto Nazionale di Geofisica e Vulcanologia, Rome, Italy, https://orcid.org/0000-0003-3489-7453 (RDS); https://orcid.org/0000-0002-5719-9909 (MGC); https://orcid.org/0000-0001-5383-7945 (PB); 2. Department of Geophysics, Graduate School of Science, Tohoku University, Sendai, Japan

*Corresponding author: raffaele.distefano@ingv.it

**Cite this article as** Di Stefano, R., M. G. Ciaccio, P. Baccheschi, and D. Zhao (2022). The Adriatic Thrust Fault of the 2021 Seismic Sequence Estimated from Accurate Earthquake Locations Using *sP* Depth Phases, *Bull. Seismol. Soc. Am.* **113**, 480–493, doi: 10.1785/0120220111

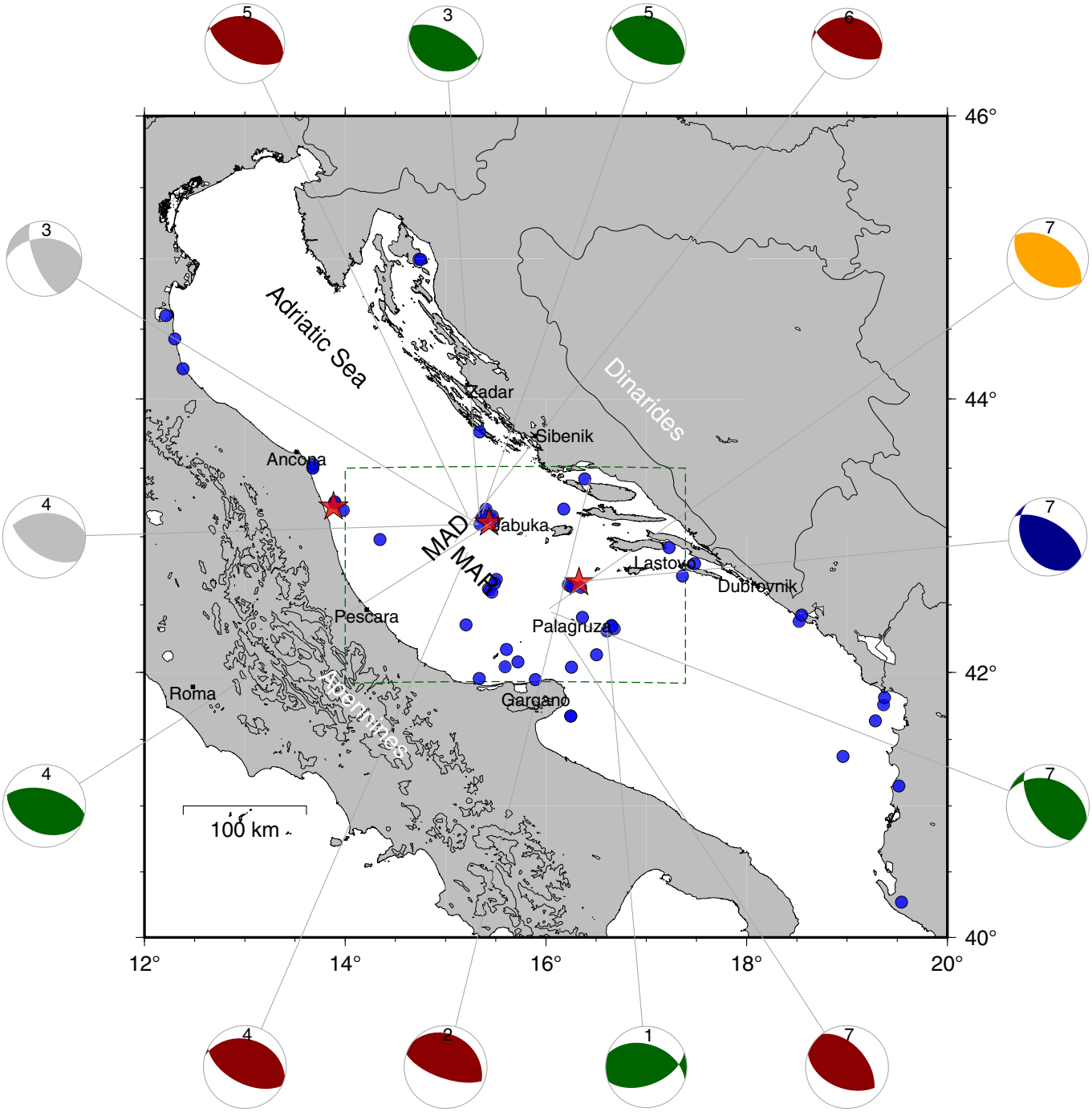


**Figure 1.** Map of the Adriatic region and seismic activity showing the locations of M ≥ 4.0 earthquakes that occurred from 1981 to 2018 (Michele *et al.*, 2017) and from 2019 to 2021 (ISIDe Working Group, 2007); both these earthquake groups were selected in the sole Adriatic offshore. The transparent blue circles represent 4 ≤ M < 5.0 earthquakes; the transparent red stars indicate M ≥ 5.0 earthquakes and the focal mechanisms from the U.S. Geological Survey (USGS) (green), Istituto Nazionale di Geofisica e Vulcanologia (INGV-regional centroid-moment tensors[RCMT]) (red), INGV/time domain moment tensor (TDMT) (purple), GEOFON (yellow), and the Croatian Earthquakes Catalog (gray) are also shown. Numbers in the focal mechanism plot indicate time ordered mainshocks: (1) 26 April 1988 $M_w$ 5.4, (2) 27 November 1990 $M_w$ 5.5, (3) 27 March 2003 $M_w$ 5.0, (4) 29 March 2003 $M_w$ 5.5, (5) 25 November 2004 $M_w$ 5.3, (6) 3 December 2004 $M_w$ 4.7, and (7) 27 March 2021 ($M_w$ 5.5 INGV/RCMT and USGS, $M_w$ 5.4 GEOFON, and $M_w$ 5.2 INGV/TDMT); the gray contours show the Italian topography at 750 m and 1500 m.a.s.l.; and the green dashed box is the target area of Figure 6. The color version of this figure is available only in the electronic edition.

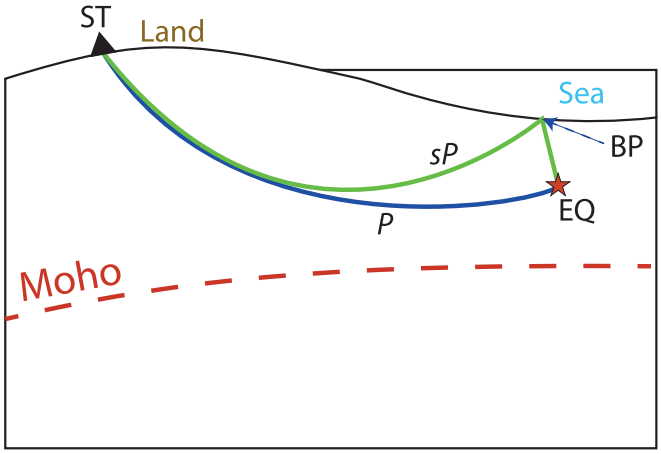


**Figure 2.** Sketch of a *sP* ray path from source to receiver, modified after Zhao *et al.* (2011); ST (black triangle) denotes station, EQ (red star) denotes earthquake, green line represents *sP* ray path, blue line represents *P* ray path, BP represents point of conversion at the sea bottom from upgoing *S* wave to downgoing *P* wave. The color version of this figure is available only in the electronic edition.

(D'Agostino *et al.*, 2008; Sani *et al.*, 2016) and highlighting the complex structural setting of this region.

Seismicity has been recorded in the central Adriatic Sea by the improving seismic network, especially in the recent decades. Despite technological improvements, the ability to obtain the precise locations of Adriatic offshore earthquakes has been hampered in both historical and instrumental seismology times due to both—the almost exclusive effects along the coast causing poor documentation and the large gaps in the distribution of seismic stations, respectively. Nevertheless, starting with the 1986–1990 seismic sequences (Console *et al.*, 1993), the Adriatic region has been viewed from a different perspective, and geodynamic investigation methods in this region have undergone new development. From the seismological point of view, however, the difficulties associated with locating hypocenters remain.

The data reported in existing seismic catalogs show remarkable seismic activity beneath the Adriatic Sea (Fig. 1), with mainshock magnitudes comparable to those recorded in the surrounding zones (Italian Seismological Instrumental and Parametric Database [ISIDe], ISIDe Working Group, 2007; Ivančić *et al.*, 2018; European-Mediterranean Seismological Center [CSEM-EMSC], Bossu *et al.*, 2008). Since 1985, the ISIDe catalog has listed six seismic events with M > 4.5 that occurred in the central Adriatic region (40 km offshore), four of which belonged to the Jabuka 2003 seismic sequence (Herak *et al.*, 2005), confirming that the seismic potential of this area is significantly higher than was assumed until some time ago. Improving our ability to locate events is thus mandatory if we are to better understand the relationship between earthquakes and the tectonic setting of this area.

It is widely reported in the literature that adding later arriving phases to *P* and *S* onsets in the relocation procedure provides stronger constraints on the earthquake's location. In particular, the use of the *sP* depth phases allows to more accurately estimate the focal depths of earthquakes compared to the use of only *P*- and *S*-wave arrivals, especially when the hypocenter is outside of a seismic network and/or the first stations is far (Umino *et al.*, 1995; Engdahl *et al.*, 1998; Zhao *et al.*, 2002; Bondár *et al.*, 2004; Engdahl, 2006; Zhao *et al.*, 2007; Zhao, 2019; Engdahl *et al.*, 2020). For example, Umino *et al.* (1995) refined the hypocentral locations of suboceanic events in the Tohoku fore-arc region using *sP* depth phase data: as a result, they revealed a double seismic zone in the Tohoku district in improved detail. The definition of the *sP* phase is as follows (e.g., Umino *et al.*, 1995, p. 357): "an upgoing *S*-wave that is subsequently reflected and converted to a *P*-wave at the top of the crust and finally reaches stations at the surface." Hence, due to the peculiar geometry of the ray path (Fig. 2), a depth phase identified in an earthquake location mimics the presence of a seismic station at the bouncing point on the local topography, thus indicating the point approximately above the hypocenter (Zhao *et al.*, 2002, 2007). The efficiency of the depth-phase arrival times in reflecting hypocenter locations resides in the fact that the travel-time difference between, for example, an *sP* phase and a *P* wave (*sP*–*P* time) mainly depends on the focal depth (Stein and Wiens, 1986; Umino *et al.*, 1995), which is approximately the segment EQ–BP in Figure 2, and on the seismic velocity structure. Thus, in the context of the Adriatic region, *sP* phases can strongly help improve the location identification of suboceanic events, therefore contributing to solving many existing controversies and open questions regarding the present-day tectonics of the Adriatic region.

## SEISMOTECTONIC SETTING OF THE CENTRAL ADRIATIC SEA

The Adriatic Sea is a mostly shallow and semienclosed elongated basin, which is an offshoot of the Mediterranean Sea (Fig. 1), on its turn part of the Tethyan margin during Mesozoic times (Dercourt *et al.*, 1986; Dewey *et al.*, 1989; Stampfli and Borel, 2002; Capitanio and Goes, 2006; Handy *et al.*, 2010).

This Adria microplate, hosting the Sea, is a northwest–southeast-trending elongated continental block surrounded by the Alpine belt, Dinaric-Hellenic systems, and Apennines belt, the formation of which began following the continental collision between the European and African plates ~40 to ~30 Ma ago (e.g., Trümpy, 1960; Coward and Dietrich, 1989; Dal Piaz, 2001; Schmid *et al.*, 2004; Handy *et al.*, 2010; Pfiffner, 2014). The Dinaric and Apennine fronts gradually migrated to the southwest and northeast direction, respectively, toward the central axis of the Adriatic Sea (Channell *et al.*, 1979). The Adriatic basin is over 800 km long and ~200 km wide (Fig. 1), and can be divided into three areas,

with increasing depths from northwest to southeast, different topographic gradients, and varying seismotectonic characteristics (Trincardi *et al.*, 1996).

The northern Adriatic Sea—a shallow and flat shelf area—has an average bottom depth of ∼35 m and occupies the flooded seaward extension of the Po Plain, representing the most extensive continental shelf in the entire Mediterranean Sea. It gently slopes down to a ∼100 m depth at the line between Pescara and Sibenik, where a slope leads to the central basin at depths of 140–150 m (Van Straaten, 1970; Trincardi *et al.*, 1996). The northern part of the basin is, by convention, bounded to the south by this transect at approximately 43.5° N.

The central Adriatic is up to 150 km wide and has an average depth of 130–150 m, but it is also characterized by the Mid-Adriatic depression (MAD)—a complex transverse depression elongated in the northeast–southwest direction for ∼125 km between Sibenik (Croatia) and Pescara (Italy), reaching depths of 240–270 m. The northern part of this region is known for seismic activity, including occurrences of relatively small earthquakes and occasional moderate earthquakes along the western coastline ($M < 5$).

Immediately to the southeast of the MAD, an aligned assembly of structural highs (the Mid-Adriatic ridge [MAR], Finetti *et al.*, 1987) extending to Palagruza has been interpreted as the result of the compressive tectonics of the external Apennines (Argnani and Frugoni, 1997; Scrocca, 2006; Scrocca *et al.*, 2007) or of the Dinaric Chains (Finetti and Del Ben, 2005); the MAR has been identified by some studies (Grandić *et al.*, 1997; Finetti and Del Ben, 2005; Geletti *et al.*, 2008) as a halokinetic structural deformation of the Burano sequence and of relatively older Triassic evaporites connected to a regional compressive regime that began in the pre-Pliocene. Some researchers (Argnani *et al.*, 1991; Calamita *et al.*, 2003) have suggested that compressive tectonics caused the inversion of some preexisting normal faults, whereas the contractional reactivation of preexisting Mesozoic normal faults from the Paleogene along the MAR has been suggested by Scisciani and Calamita (2009) and Gambini *et al.* (1997).

The central Adriatic Sea is separated from the southern area by a line that runs from the Gargano Peninsula to the Croatian coast (the Gargano–Dubrovnik line). The southern area shows a wide depression with depths ranging from 1218 to 1225 m.

According to the ISIDe Catalog (ISIDe Working Group, 2007), the Adriatic area exhibits moderate-to-strong seismicity (Fig. 1). The central part is the most active region of the Adriatic platform, with $M_L$ (local magnitude) ≥5.0 events occurring over the last 30 yr, suggesting that the seismic potential of this area is significantly higher than assumed in the past. Along the Central Adriatic coast, two main seismic sequences have occurred. The first occurred in 1987, with an $M_L$ of 5.0, characterized by a compressive fault solution. This sequence was located very close to the Adriatic coast—40 km south of Ancona (Riguzzi *et al.*, 1989).

A second sequence occurred in 2013 in the Conero offshore region, with an $M_w$ (moment magnitude) 4.9 mainshock also characterized by a compressive focal mechanism (see Data and Resources for details). This sequence occurred approximately 20 km from the city of Ancona. Regarding the Central Adriatic offshore region, the strongest earthquakes have occurred in the open sea area, with the earthquakes of the 2003 Jabuka seismic sequence (Herak *et al.*, 2005), the 1988 Palagruza seismic sequence (Herak *et al.*, 1996), and the 2021 seismic sequence analyzed in this article reaching magnitudes up to $M_w$ 5.5. The focal mechanisms of these mainshocks, aligned along the northwest–southeast direction, are shown in Figure 1.

The mainshock of the 2021 seismic sequence occurred approximately 20 km north of the Palagruza Islands, 80 km from the Gargano promontory, and approximately 40 km from the Croatian island of Lastovo. This mainshock was felt in many central–southern Italian regions, from Ancona to Foggia, and in Central Dalmatia. The epicenters occurred in the open sea, approximately 100 km southeast of the 2003 Jabuka seismic sequence and approximately 50 km northwest of the 1988 Palagruza seismic sequence. The corresponding hypocenters' alignment dipped northeast, like the fault system identified using the available seismicity and reflection profiles in the area (Herak *et al.*, 2005; Geletti *et al.*, 2008, 2020; Grandić *et al.*, 2010; Peace *et al.*, 2012; and references therein), thus placing the seismic sequence on the Dinaric front. The fault-plane solution of the 2021 mainshock derived based on the time domain moment tensor (TDMT, Fig. 1, number 7, red) solution indicates faulting caused by northeast–southwest-oriented tectonic compression on a reverse fault. The seismicity in the Croatian offshore region near Jabuka Island should be linked to a northwest–southeast-trending external thrust fault of the Dinaric Chain (Herak *et al.*, 2005).

## DATA AND METHODS

To analyze this seismic sequence in detail, we selected 80 $M_L \geq 2.9$ earthquakes that occurred from 27 March 2021 to 30 September 2021 from the Istituto Nazionale di Geofisica e Vulcanologia (INGV) catalog (ISIDe Working Group, 2007; see the INGV webservices in Data and Resources) within 50 km of the epicenter of the mainshock ($M_w$ 5.2) that occurred on 27 March 2021. We then downloaded the three-component seismograms recorded at stations within 300 km of these earthquakes from the INGV bulletin hypocenter using the INGV European Integrated Data Archive (EIDA) node (Strollo *et al.*, 2021, and references therein) INGV webservice. Finally, we visually analyzed the waveforms to identify the *P*-, *S*-, and *sP*-wave onsets.

Although *P*- and *S*-wave arrivals are present in a waveform, whether they are visible or not, the *sP* onset can be either completely absent or difficult to discriminate with respect to other possible reflections. Nevertheless, the previous studies (Umino and Hasegawa, 1994; Umino *et al.*, 1995; Zhao *et al.*, 2002, 2011;

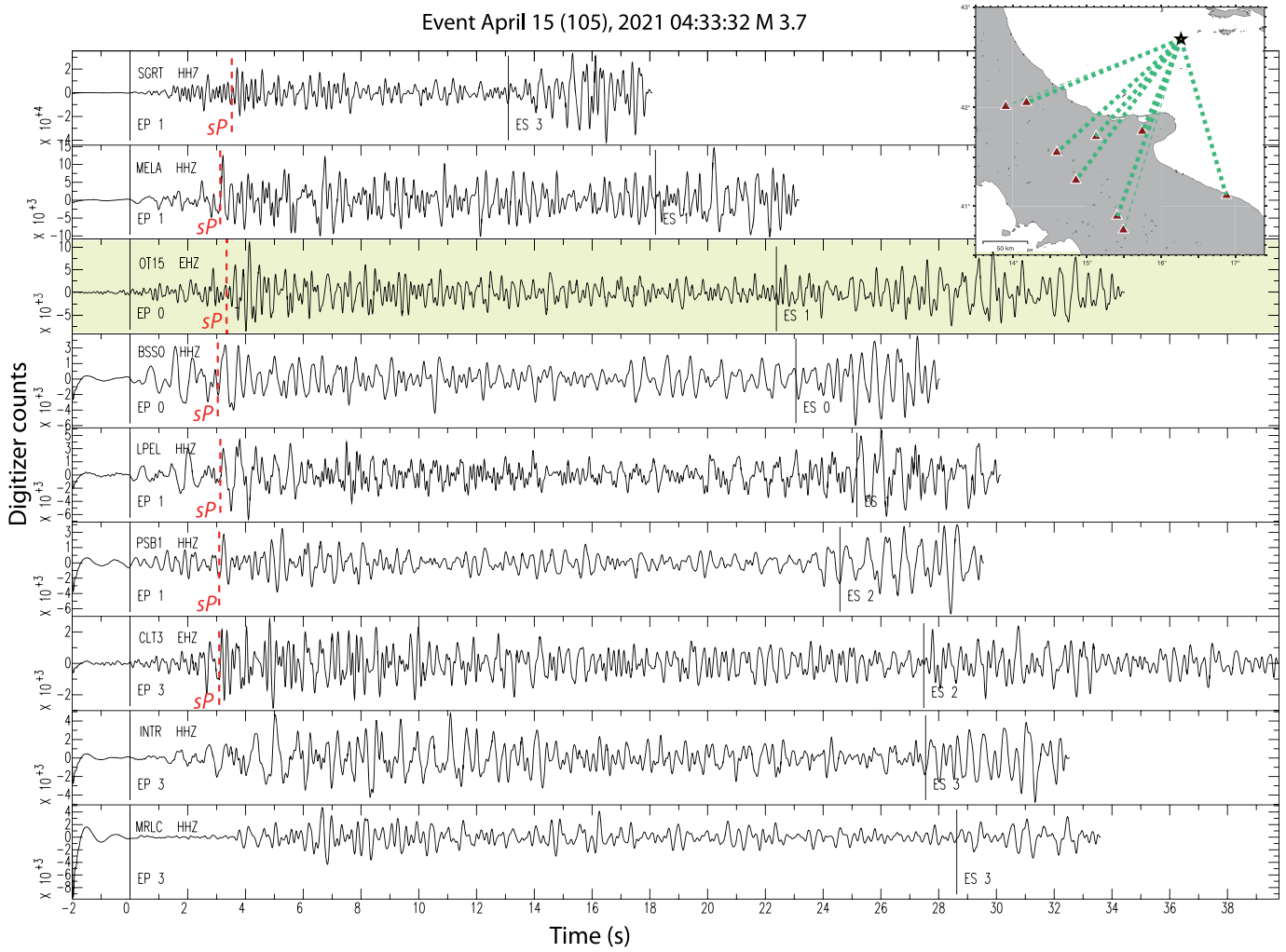


Gamage *et al.*, 2009; Huang and Zhao, 2013a,b; Liu *et al.*, 2013a, b) have defined important guidelines for detecting *sP* phases.

We thus built a workflow in seven subsequent points to identify *sP* onsets and locate events: (1) station file integration, (2) waveforms cut, (3) *P* + *S* picking, (4) waveforms stacking, (5) *sP* picking, (6) *sP* confirmation by particle motion, and (7) earthquake location. The first part of this workflow was based on two key points: (1) the *sP* phase is a conversion from an up-dipping *S* wave to a down-dipping *P* wave, and its vertical-component signal is thus typically stronger than its horizontal-component signal; and (2) on a record section for a single event at different stations, with *P*-onset-aligned waveforms, the *sP*–*P* differential time is nearly a constant, exhibiting only small variations related to the 3D structure of Earth. This latter feature results from the up-dipping part of the *S* ray, from the hypocenter to the surface topography (the segment EQ–BP in Fig. 2), depending only on the real focal depth, whereas the second part, the *P* ray moving from the conversion point at the surface to the receiver (BP and ST, respectively in Fig. 2), especially at distances beyond 90–150 km, is similar to a direct *P* wave (EQ–ST in Fig. 2). Thus, the *sP* delay at these distances is due almost entirely to the focal depth. Hence, our first step, after manually identifying the *P*- and *S*-wave onsets, was to produce vertical-component waveform stacks aligned on the *P* onsets. Stacking all the waveforms is important, because it strongly highlights alignments of similar signals at different stations. This is of great help in identifying a group of stations where a possible *sP* wavelet is visible at an almost constant delay time following the *P*-wave onset (see Fig. 3). Then, among these stations, we chose usually no more than two of the clearest onsets, that is to say only those (even only one) to which we can attribute full weight. We discard the others, as discussed in Zhao *et al.* (2011), because *sP* is a very strong constraint for depth in the location code, so the use of *sP* onsets with higher uncertainty would only add noise to the

**Figure 3.** Example of vertical components waveforms of the event 15 April 2021 $M_L$ 3.7 T04:33 aligned on the *P* onsets; the red dashed lines denote possible *sP* onset on different waveforms, in this case at about 3 s after the *P* onset; the yellow highlighted waveform hosts the chosen *sP* onset, at station OT15. Inset: The red triangles, the star, and the green dashed lines are the seismic stations recording the traces shown in the figure, the location of the reported earthquake, and the projection of the ray-paths at surface, respectively. The color version of this figure is available only in the electronic edition.

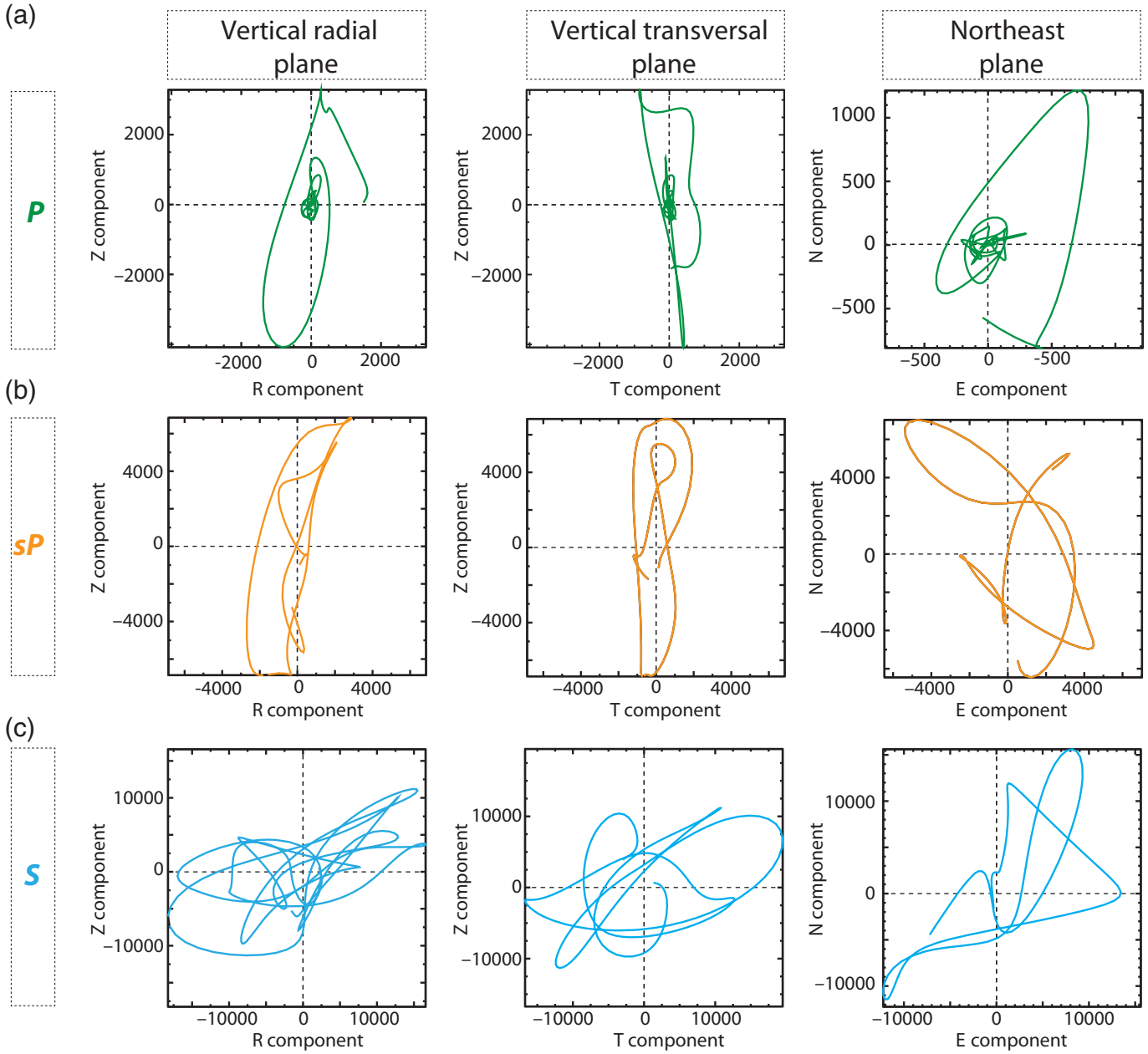


**Figure 4.** An example of particle motions of (a) *P*- (green), (b) *sP* (orange), and (c) *S* onset (sky-blue) on the vertical–radial (column 1), vertical–transverse (column 2), and north–east (column 3) planes for the 27 March 2021 $M_L$ 4.1 T14:01 aftershock at station BSSO. The color version of this figure is available only in the electronic edition.

inverse problem. A third important feature is that the particle motion of an *sP* phase is quite similar to that of a *P* wave, because the EQ–ST segment of the seismic ray (Fig. 2) travels and hits the seismic station as a *P* wave with a long-distance geometry almost equal to that of the direct *P* wave. We thus performed a particle motion analysis on the identified possible *sP* wavelets and removed those that did not respond to this feature from the set (see Fig. 4). Finally, we used the on-purpose code designed by Zhao *et al.* (2007, 2011) to accurately locate the earthquakes. This code uses theoretical information computed with its advanced 3D ray tracer for the *P*, *S*, and *Pn* waves, *Sn* waves refracted at the Moho interface as well as for the *sP* waves converted at the surface, to better constrain the absolute 3D event position. To simplify as much as possible our first approach to analyzing the Adriatic earthquakes and to cope with the small local scale, we chose to use crustal and mantle *P*- and *S*-wave velocities from a 1D mean local velocity model based on a high-resolution large-scale 3D regional model. We extracted the 1D velocity model (Fig. S1, available in the supplemental material to this article), applying a trilinear interpolation method from the more recent 3D *P*- and *S*-wave velocity model developed by Magnoni *et al.* (2022). This model is particularly detailed in the Italian offshore regions with respect to the previous ones.

To allow the code to properly model the *P*- and *S*-wave refractions at the Moho, we introduced the latest Moho topography derived by Di Stefano *et al.* (2011). The location code by Zhao *et al.* (2007, 2011) combines the crustal and mantle *P*- and *S*-wave velocities from the 1D model with the Moho topography, to apply Snell's law at the seismic interface. Finally, as the surface conversion at the BP (Fig. 2) is usually controlled by the sediment thickness and the surface topography, we also added this information as input of the location code. Nevertheless, in the specific Adriatic subregion where the seismic sequence analyzed in this article occurred, the sediments are quite thin. Thus, in our first approach, we used a constant 0.1 km thick layer, a *P*-wave velocity ($V_P$) of 1.8 km/s, and a $V_S$ of 0.6 km/s across the whole region to model the sedimentary layer; we based this relatively strong approximation on a comparison between the previous studies on the sediments in the Adriatic region (Trincardi *et al.*, 2004; Giustiniani *et al.*, 2020; Vrdoljak *et al.*, 2021).

## RESULTS

We obtained hypocentral parameters of 70 earthquakes from the March 2021 seismic sequence by reliably identifying at least one *sP* onset per earthquake. Figure S2 reports hypocentral location uncertainties (linear inverse problem estimated standard errors from the location code) and intrinsic (azimuthal gap and distance of the closest station) quality statistics. Notably, we did not select waveforms from stations within the Dinaric-side networks. The waveforms from the Croatian network are not openly available yet, whereas the few others, to northeast and southeast, though they would slightly reduce the gap, are too far to be of any help constraining the focal depth. We then, on purpose, decided to use a uniform approach to the whole sequence, selecting only those stations within no more than 300 km distance independently from the GAP. This approach resides on the strength of the method that we are using that allows us to constrain the focal depth by using *sP* onsets, as explained in the previous sections. The location method was, in fact, designed to deal with "large" gap conditions. This situation is reflected by the gap distribution histogram (Fig. S2) reporting an azimuthal gap ≥ 240°. In addition, the distribution of the distances between the first stations and the final epicenters is a consequence of the offshore (off-network) earthquake positions, as no stations were located above the hypocenters. The formal hypocenter errors were quite low with respect to typical offshore events, generally smaller than 2–3 km; these values are very close to the errors expected for absolute locations of events that occur beneath seismic networks.

Figure S3 shows the origin time uncertainties versus longitude, latitude, and focal depth uncertainties. Here, we can observe a classic trade-off between the focal depth and origin time. However, it is important that this trade-off, which is usually much larger when locating focal depths in off-network events, is essentially spatially isotropic in this case, suggesting that the use of the *sP* phase greatly helps reduce hypocentral mislocations and uncertainties.

In the inset of Figure 5, we report the observed *sP–P* delay times (circles) as a function of the relocated hypocenters' depth. The time distance of *sP*-arrival times from *P*-arrival times approximately grows with growing hypocenter depth in agreement with observations from the previous studies (Umino *et al.*, 1995). Nevertheless, we observe variability. The slight dispersion is most likely due to the 3D heterogeneity of the real Earth structure based on hypocenter and station relative position.

Figure 5 shows the number of *sP* observations selected per station against the corresponding station positions on a map. Although we only selected the best *sP* onset records on purpose, we did select records for all events. Thus, Figure 5 is quite representative of the stations at which high-quality *sP* phases were observed most of the time. The station IV MOCO, showing the highest number of best observations, is located at a mean distance of ∼170 km from the seismic sequence at an elevation of approximately 1 km a.s.l. Moreover, a relatively high number of *sP* phases were also observed at shorter epicentral distances along the same azimuth. Despite this evidence, and those from the inset of Figure 5, our dataset was not sufficiently large or statistically significant to assess the reason for these higher or lower *sP* visibilities at specific sites, and *sP–P* delays distribution.

Figure S4 shows the *sP* residuals derived for the whole dataset with respect to the formal focal depth and epicentral location errors. This analysis showed no significant trends between these variables, especially regarding the focal depth and related uncertainty, except for the origin time uncertainty, for which smaller errors seemed to correspond to smaller *sP*-residual spreading. This result indicates that the use of *sP* phases can help reduce the typically strong trade-off effect between the focal depth and origin time as well as the associated uncertainties.

In Figure S5a, we report the locations from the INGV Bulletin (manually revised picks and locations) and CSEM (automatic routine locations) agencies for the Adriatic 2021 seismic sequence, all compressed in one single vertical section corresponding to trace and vertical section "b" of Figures 6 and 7, respectively. When compared to Figure 7, this image shows almost flat alignments of hypocenters around ∼10 km depth for both the agencies. In addition, we report in Figure S5b, d, the distribution of azimuthal gap for INGV and CSEM, and formal horizontal errors of the only INGV agency (these values are not available from the CSEM webservice QuakeML). INGV formal horizontal errors are strongly influenced by the fixed depth approach. Vertical errors from both INGV and CSEM are conversely not available for most of the analyzed earthquakes due to the "fixed depth" option. Both the flat alignments and the need for the fixed depth option, despite

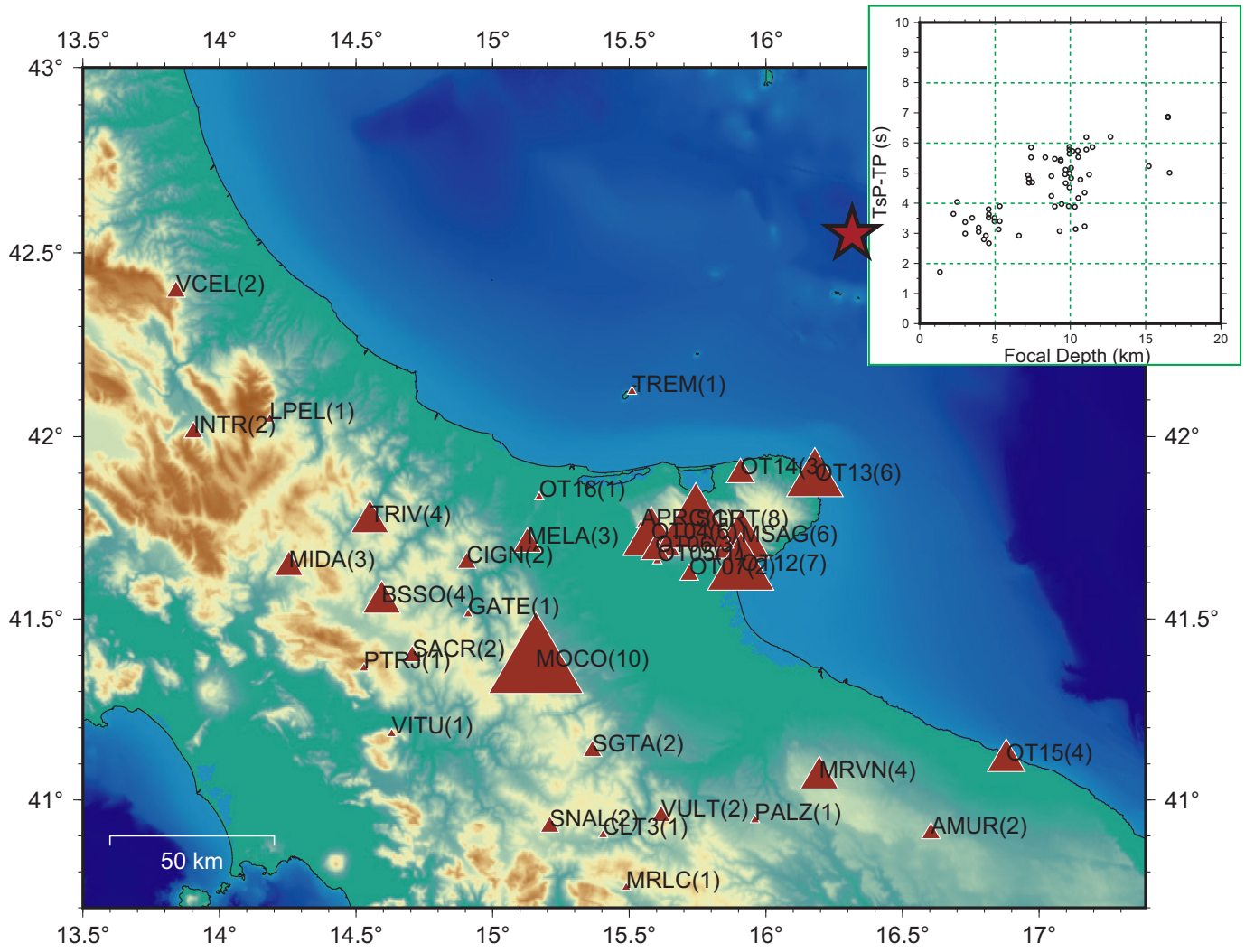


**Figure 5.** Distribution of the seismic stations (dark red triangles) used in this study. The size of each triangle is proportional to the number of *sP* arrivals, reported among brackets, observed at the corresponding station. The red star denotes the epicenter of the $M_w$ 5.2 earthquake that occurred on 27 March 2021 and the gray and green contour lines show the 750 m/1500 m.a.s.l. topography and bathymetry with 50 m.b.s.l. step, respectively. The inset reports the observed *sP–P* times versus focal depths (black open circles). The color version of this figure is available only in the electronic edition.

the smaller azimuthal gaps, are expected due to the large epicentral distances of the closest stations, which is exactly what the use of *sP* helps to solve.

Finally, to further demonstrate the improvements introduced in this article using *sP* observations, we performed a relocation of the same selected 70 earthquakes, using a traditional location approach with only *P* + *S* readings but in the same local best 1D model used in the present work. First, we downloaded high-quality readings manually revised by the analysts seismologists of INGV and relocated them with the classical widely used Hypoellipse location code (Lahr, 1999) with optimized configuration (e.g., epicentral distance cut is kept high to reduce the gap with far stations). Then we removed *sP* from our readings dataset, and we ran again the Zhao *et al.* (2007, 2011) location code used in the present article. The results of this test are reported in Figure S6 along the same vertical sections of Figure 7. In both the cases, approximately half of the earthquake locations did not converge to a solution unless the depth was fixed. The final seismicity distribution from these two classical location tests differs from each other and from Figure 7. In addition, neither of the two test distributions identify any consistent and reliable alignment. Most of the earthquakes are organized in sparse vertical or horizontal clusters. This further confirms the relevance of using the *sP* phases, able to strongly constrain the earthquake's depth mimicking the presence of a receiver "on top" of the hypocenter.

## DISCUSSION

Between March and September 2021, a total of 80 earthquakes (M ≥ 2.9) were recorded in the Central Adriatic Sea within the Adria microplate. The seismic sequence started with the mainshock on 27 March 2021, at 13:47:51, with $M_w$ 5.2 according to INGV ($M_w$ 5.5: U.S. Geological Survey [USGS]; $M_w$ 5.4:

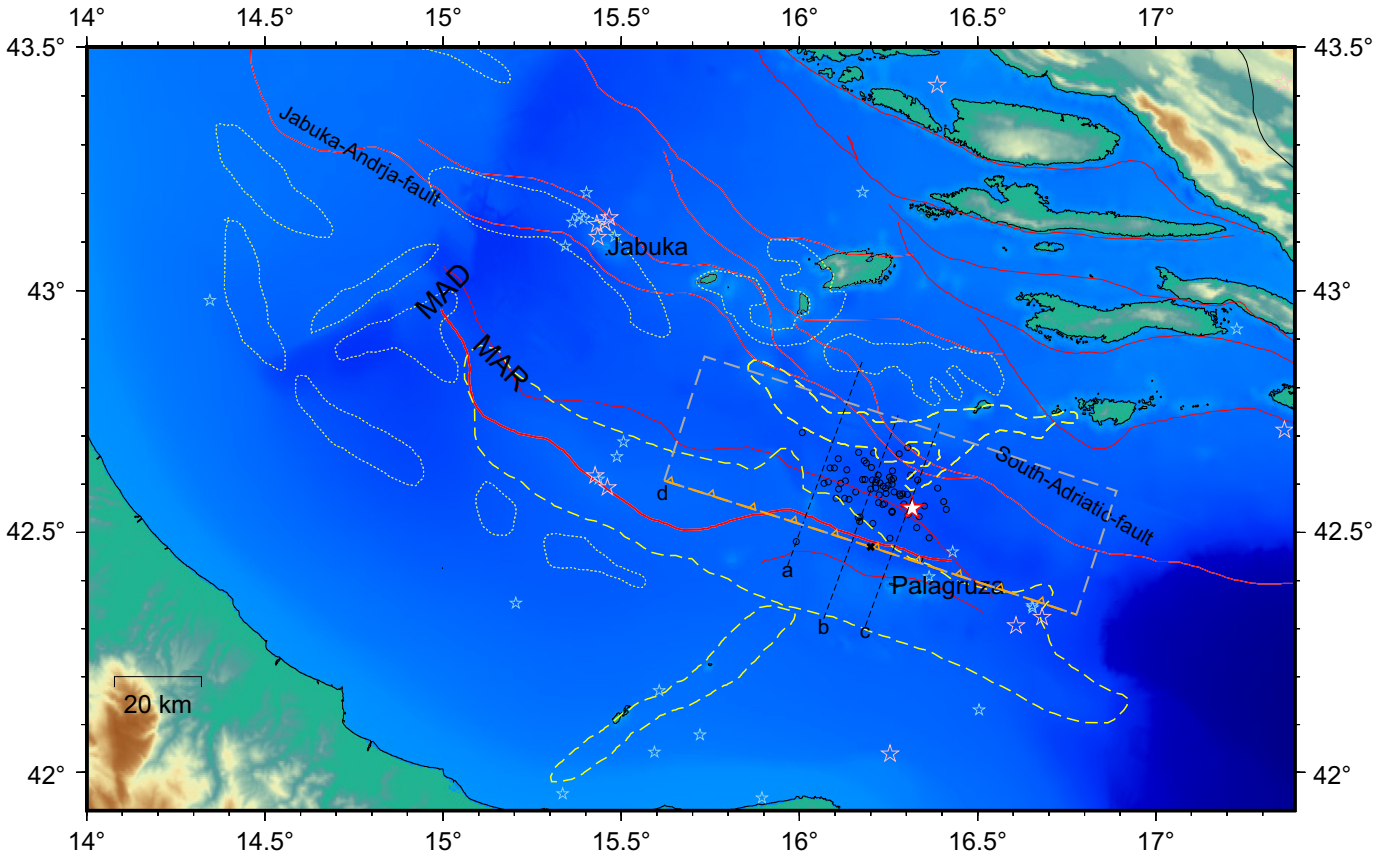


**Figure 6.** Map of the central Adriatic area. The light blue and pink stars denote M > 4 and 5 events, respectively, as collected from Michele *et al.* (2017) and Italian Seismological Instrumental and Parametric Database (ISIDe) (ISIDe Working Group, 2007). The red lines denote active faults (Ivančić *et al.*, 2006). The yellow dashed lines are the larger halokinetic structures reproduced from Geletti *et al.* (2020): thicker lines are the two structures reported in the vertical sections "a–c" in Figure 7. MAR, the Mid Adriatic ridge (Finetti *et al.*, 1987) or the Central Adriatic Deformation Belt (Argnani and Frugoni, 1997). MAD, the Mid-Adriatic depression (Geletti *et al.*, 2008, and references therein). The light-to-dark tones of blue represent shallow-to-deep water. The red star and black open circles represent the 2021 mainshock ($M_w$ 5.2) and its aftershocks, respectively, as located in this study. The three black dashed lines denote the locations of the vertical cross sections shown in Figure 7a–c. The gray dashed box and the orange dashed line "d" represent the modeled fault-plane projection (Figure 7d) and its surface trace, with the triangles pointing toward the dip direction. The color version of this figure is available only in the electronic edition.

GEOFON). Figure 6 shows that the epicenters are located along a seismically active northwest–southeast-trending area between the 2003 Jabuka seismic sequence to the northwest and the 1988 Palagruza seismic sequence to the southeast. The distribution of these epicenters corresponds to the fault traces discussed in Ivančić *et al.* (2006), somewhat characterized by an inverse rupture mechanism. Despite the identification of this rupture mechanism, a clear image of the fault geometries throughout the whole area is difficult to derive based on the earthquake depth distribution (Herak *et al.*, 2005) due to difficulties in constraining offshore hypocentral locations that lack nearby seismic stations. Conversely, using the *sP* phase to constrain the focal depth, and consequently the latitude and longitude information, as we did in the present work, results in a quite clear image of the fault geometry associated with the 2021 seismic sequence; hereafter, we call this fault geometry the Mid-Adriatic fault (MAF).

Figure 7 shows four vertical sections across the strike of the $M_w$ 5.2 fault. The southwest–northeast-oriented cross sections (Fig. 7a–c) show a clear dip to the northeast. The mainshock is located approximately in the middle of the aftershock zone, ranging from depths close to the bathymetry to a ~20 km depth along the fault plane. Based on the hypocentral distribution, this fault shows a northeastward dip between ~35° and ~45°, within the range of the moment tensor solutions determined by different institutions (Fig. 1). The MAF runs southwest and parallel to the Jabuka–Andrija fault and South Adriatic fault (see Ivančić *et al.*, 2006; Kastelic *et al.*, 2013) and along the northwest–southeast-trending alignment of structural highs called the MAR (Fig. 6) (Finetti *et al.*, 1987). We modeled the mean fault plane based on the 3D earthquake alignment. The gray box in Figure 6 and the gray line in Figure 7a–c represent the modeling results. Following this geometry, we constrained the fault outcrop at the seafloor with a mean dip of ~35°, corresponding to the fault segment reported in the Map of Active Faults published by Ivančić *et al.*

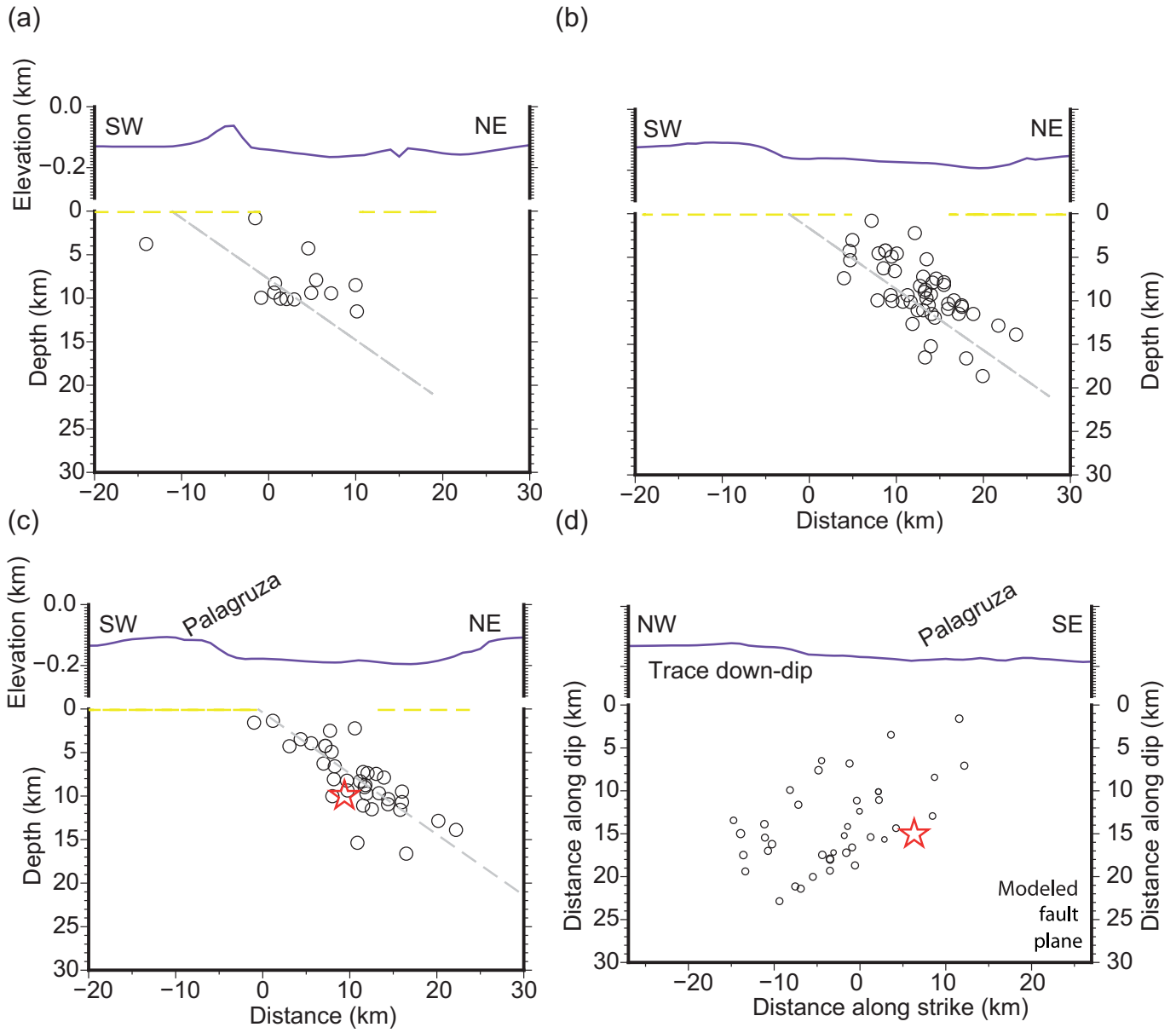


(2006, and references therein), where the fault segment was shown with unknown displacement direction.

The MAR appears to be a key feature in the seismotectonic setting of the study area. This ridge was interpreted as a forebulge by De Alteriis (1995) and has also been reported to be the result of compressive tectonics of the external Apennine (Argnani and Frugoni, 1997; Scrocca, 2006; Scrocca *et al.*, 2007) or Dinaric (Finetti and Del Ben, 2005) chains. According to Grandić *et al.* (1997), the two main MAR alignments—the Palagruza High and the Jabuka ridge—were caused by salt doming of Triassic evaporites. This halokinetic tectonic process, which is still active, characterizes sectors in which successive regional compressive regimes induce reduced resistance to deformation, leading to the formation of preferential pathways for gas-rich fluid extrusion from the sedimentary sequences to the seafloor and shallow areas below the sea bottom where these gas seepages appear as pockmarks, mud volcanoes, and mud-carbonate mounds (Geletti *et al.*, 2008).

**Figure 7.** (a–c) Vertical cross sections showing the hypocentral distributions along the three profiles shown in Figure 6. The open circles denote M < 5 earthquakes, whereas the red star denotes the mainshock ($M_w$ 5.2) that occurred on 27 March 2021. The gray dashed line denotes the mean modeled 35° dipping plane. The yellow dashed lines are the traces of the halokinetic structures from Geletti *et al.* (2020), reported in Figure 6. (d) Distribution of earthquakes' hypocenters that occurred within 3 km of the modeled dipping plane, as shown in panels (a–c) and in Figure 6, gray dashed box. The color version of this figure is available only in the electronic edition.

Our results indicate that the structure activated during the 2021 seismic sequence outcrops close to the Palagruza High. The previous studies have suggested halokinetic activity

occurring in this area, in the framework of compressive or transpressive tectonics interacting with the migration of gas-rich fluids (Geletti *et al.*, 2008, 2020, and references therein). The bathymetry, also reported in the upper side of the vertical sections (Fig. 7a–c), draws two scarps to the southwest and to the northeast of the Adriatic fault—consequences of the salt doming deforming the seafloor (Geletti *et al.*, 2020). The 2021 seismicity reported on these vertical sections is located in between two of the larger halokinetic zones. In particular, the southwest salt structure is located in the footwall of the fault, which probably causes or facilitates its upward propagation. Further studies will be necessary to analyze the correlations between these active compressional structures. Figure 7d shows an "along-plane" down-dipping section consisting of earthquakes located within ±3 km of the modeled fault plane. This plot represents the distribution of the located earthquakes on the fault plane and seems to show that the northernmost, shallow fault region was not completely activated or may be locked. However, this possibility should be further confirmed by extending the dataset temporally and lowering the magnitude of completeness.

Another important aspect of correctly mapping the faults responsible for offshore Adriatic events involves the corresponding tsunami hazard. The Adriatic Sea has been struck by tsunamis several times in the past (Tinti *et al.*, 2004; Maramai *et al.*, 2019) (see also Paulatto *et al.*, 2007 for a complete review). Although the northwestern Adriatic Sea is particularly vulnerable due to the extremely shallow water present in that region, the central and southern parts are also exposed to such risks as was well documented in Stoppa (2014), who analyzed the 1627 M 6.7 Frentana coast earthquake (~200 km west of the MAF, in the Abruzzi coastal region) and the related tsunami, the destructive effects of which have been historically confirmed. Stoppa (2014) stressed this risk and expected the development of rapid tsunami propagation modeling regarding the eventuality that a moderate-to-strong earthquake would occur in Adriatic coastal or offshore areas. Recently, INGV has developed the Tsunami Alert Center, which is part of the large global community for tsunami monitoring and early warning (Selva *et al.*, 2021, and references therein). Beyond the complexity of tsunami modeling, the wavefront propagation probability analysis method and the alert system itself are based on some criteria regarding the tsunamigenic potential, and a relevant component of this potential is the focal depth of the earthquake triggering the tsunami and the possible extension of the fault slip to the surface. In this sense, our analysis of the 2021 seismic sequence suggests that the MAF, although previously related to moderate events with magnitudes smaller than the minimum M 5.5 threshold for the Decisional Matrices, might produce ruptures that propagate to the seafloor in the future, thus increasing the already-evidenced tsunamigenic potential (Stoppa, 2014) of Adriatic faults and, in general, of this large, seismically active area.

## CONCLUSIONS

The 2021 central Adriatic seismic sequence activated a segment of an active fault system located in the central offshore Adriatic Sea region along the axis of the Adria microplate involved in a double-verging subduction environment. The tectonics of this area are determined by the migration of the outer thrusts of the Apennines and External Dinarides toward the northeast and southwest, respectively, generating a compressive regime that has led to a complex system of northwest–southeast-trending thrust faults, back thrusts, and anticlines and to important halokinetic structure and vertical uplifting alignments. This analysis of instrumental seismicity shows that the several faults identified using active-source seismology in the framework of petroleum and gas exploration in this area are anything but seismically inactive or poorly active, despite the moderate magnitudes of the relatively strong events, thus confirming the suggestion of Kastelic and Carafa (2012).

In the present work, we analyzed seismograms recorded at inland stations with regard to the earthquakes that occurred during March and September 2021 in the central Adriatic Sea, thus identifying a set of high-quality *sP* onset records that were added to the canonical *P* and *S* onsets. We then applied the offshore earthquake locating method developed by Zhao *et al.* (2007, 2011). Despite the absence of close-to-epicenter stations, this approach allowed us to better constrain the hypocentral locations, especially the focal depths of the earthquakes, thus allowing us to more accurately associate the seismic sequence with a specific fault and providing fault geometry information.

Our results suggest that the 2021 central Adriatic seismic sequence occurred along a northeast-dipping fault, which we called the MAF. This fault has already been identified in seismic exploration studies, although it was previously reported to have an "unknown vergence direction" (Ivančić *et al.*, 2006, 2018). This fault segment is located parallel to and between the 2003 Jabuka and 1988 Palagruza seismic sequences to the northwest and southeast, respectively, in an area that previously did not show high-rate seismicity. The TDMT associated with the 2021 mainshock shows a thrust-fault mechanism. Our results suggest that this seismic sequence activated the MAF from near-surface depths to a depth of approximately 20 km, with the mainshock located approximately in the middle of this sequence zone. Despite the high accuracy of the hypocentral locations, we constrained the dip angle within a range of 35°–45°; this range is compatible with a thrust fault and is within the range resulting from moment tensor analyses by several seismic monitoring agencies; however, our results exhibit some variation from the slightly higher TDMT. The hypocentral distribution revealed in this study is in very good agreement with the MAF trace at the surface, and both the position and strike of this fault are near the uprising halokinetic structures, thus confirming the correlation between these geological features and seismic activity in the central Adriatic crustal region. Precisely identifying

the geometries of the active faults that are responsible for the moderate-to-possibly strong earthquakes under the Adriatic Sea is also relevant when studying the tsunamigenic potential of seismic sources in coastal areas that are prone to tsunami-related damages. We also believe that our results are very promising for constructing a map of offshore seismicity in Italy with an improved accuracy. Our next step will be to further improve the accuracy of the hypocentral locations derived herein by adding more detailed a priori information regarding the local 1D, or even 3D, crustal velocity models and the sedimentary cover. Moreover, we will progressively apply the *sP* identification and earthquake-locating methods utilized herein to assess as many offshore seismic sequences in the Adriatic, Ionian, and Tyrrhenian seas as possible, with the aim of increasing the routine utilization of this approach in Italy.

## DATA AND RESOURCES

The waveforms analyzed in this article are available through the European Integrated Data Archive (EIDA) webservices (https://www.orfeus-eu.org/data/eida/webservices/); the hypocentral locations discussed in the present article and shown in Figures 6 and 7 are available in the supplemental material in the form of a "Comma Separated Values (.csv)" file. Data from CSEM are available at https://www.seismicportal.eu/fdsnws/event/1/; data from Istituto Nazionale di Geofisica e Vulcanologia (INGV) are available at http://webservices.ingv.it/fdsnws/event/1/. Details of the 21 July 2013 03:32:24 $M_w$ 4.9 event, mentioned in the Seismotectonic setting of the central Adriatic sea section, can be found at http://terremoti.ingv.it/event/2367191. The supplemental material for this article includes six figures (1D *P*- and *S*-velocity model, analysis of the locations quality parameters, locations form regional agencies, test locations with only $P + S$ arrivals), and the catalog of the locations with *sP* arrivals produced and analyzed in this article in "Comma Separated Values".csv file. All websites were last accessed in November 2022.

## DECLARATION OF COMPETING INTERESTS

The authors acknowledge that there are no conflicts of interest recorded.

## ACKNOWLEDGMENTS

The authors appreciate the helpful discussions with Lucia Margheriti, Z. Huang, X. Liu, and G. Toyokuni. The editor and two anonymous reviewers provided thoughtful review comments and suggestions, which have greatly improved this article. Most of the figures are made with the Generic Mapping Tools (GMT) Version 6 (Wessel *et al.*, 2019). Funding was provided by the FASTMIT (FAglie Sismogeniche e Tsunamigeniche, D52F16001150001) "Premiale 2014" of the Italian Ministry of Infrastructure. This work was partially supported by a research grant (Grant Number 19H01996) provided to D. Zhao by the Japan Society for the Promotion of Science.

## REFERENCES

Argnani, A., and F. Frugoni (1997). Foreland deformation in the Central Adriatic and its bearing on the evolution of the Northern Apennines, *Ann. Geophys.* **40,** no. 3, 771–780.

Argnani, A., A. Artoni, G. G. Ori, and M. Roveri (1991). L'avanfossa centro-adriatica: Stili strutturali e sedimentazione, *Studi Geologici Camerti*, Special Issue, 1991/1, 371–381 (in Italian).

Bondár, I., S. C. Myers, E. R. Engdahl, and E. A. Bergman (2004). Epicenter accuracy based on seismic network criteria, *Geophys. J. Int.* **156,** 483–496.

Bossu, R., G. Mazet-Roux, V. Douet, S. Rives, S. Marin, and M. Aupetit (2008). Internet users as seismic sensors for improved earthquake response, *Eos Trans. AGU* **89,** 225–226.

Calamita, F., W. Paltrinieri, M. Pelorosso, V. Scisciani, and E. Tavernelli (2003). Inherited Mesozoic architecture of the Adria continental paleomargin in the Neogene central Apennines orogenic system, Italy, *Boll. Soc. Geol. Ital.* **122,** 307–318.

Capitanio, F. A., and S. Goes (2006). Mesozoic spreading kinematics: Consequences for Cenozoic Central and Western Mediterranean subduction. *Geophys. J. Int.* **165,** 804–816, doi: 10.1111/j.1365-246X.2006.02892.x.

Channell, J. E. T., B. D'Argenio, and F. Horváth (1979). Adria, the African promontory, in mesozoic Mediterranean palaeogeography, *Earth Sci. Rev.* **15,** no. 3, 213–292, doi: 10.1016/0012-8252(79)90083-7.

Console, R., R. Di Giovambattista, P. Favali, B. W. Presgrave, and G. Smriglio (1993). Seismicity of the Adriatic microplate. *Tectonophysics* **218,** 343–354.

Coward, M., and D. Dietrich (1989). *Alpine Tectonics—An Overview*, Vol. 45, Geological Society, London, Special Publications, London, United Kingdom, 1–29, doi: 10.1144/GSL.SP.1989.045.01.0.

D'Agostino, N., A. Avallone, D. Cheloni, E. D'Anastasio, S. Mantenuto, and G. Selvaggi (2008). Active tectonics of the Adriatic region from GPS and earthquake slip vectors, *J. Geophys. Res.* **113,** 1–19, doi: 10.1029/2008JB005860.

Dal Piaz, G. V. (2001). History of tectonic interpretations of the Alps, *J. Geodynam.* **32,** nos. 1/2, 99–114.

De Alteriis, G. (1995). Different foreland basins in Italy: Examples from the central and southern Adriatic Sea, *Tectonophysics* **252,** 349–373.

Dercourt, J., L. P. Zonenshain, L. E. Ricou, V. G. Kazmin, X. Le Pichon, A. L. Knipper, C. Grandjacquet, I. M. Sbortshikov, J. Geyssant, C. Lepvrier, *et al.* (1986). Geological evolution of the Tethys belt from the Atlantic to the Pamirs since the Lias, *Tectonophysics* **123,** 241–315.

Dewey, J. F., M. L. Helman, E. Turco, D. H. W. Hutton, and S. D. Knott (1989). Kinematics of the western Mediterranean, in *Alpine Tectonic*, M. P. Coward and D. Dietrich (Editors), Vol. 45, Geological Society Special Publication, London, United Kingdom, 265–283.

Di Stefano, R., I. Bianchi, M. G. Ciaccio, G. Carrara, and E. Kissling (2011). Three-dimensional Moho topography in Italy: New constraints from receiver functions and controlled source seismology, *Geochem. Geophys. Geosys.* **12,** Q09006, doi: 10.1029/2011GC003649.

Engdahl, E. R. (2006). Application of an improved algorithm to high precision relocation of ISC test events, *Phys. Earth Planet In.* **158,** no. 1, 14–18, doi: 10.1016/j.pepi.2006.03.007.

Engdahl, E. R., D. GiacomoDi, B. Sakarya, C. G. Gkarlaouni, J. Harris, and D. A. Storchak (2020). ISC-EHB 1964–2016, an improved data set for studies of Earth structure and global seismicity, *Earth Space Sci.* **7,** e2019EA000897, doi: 10.1029/2019EA000897.

Engdahl, E. R., R. van der Hilst, and R. Buland (1998). Global teleseismic earthquake relocation with improved travel times and procedures for depth determination, *Bull. Seismol. Soc. Am.* **88,** no. 3, 722–743, doi: 10.1785/BSSA0880030722.

Finetti, I., G. Bricchi, A. Del Ben, M. Pipan, and Z. Xuan (1987). Geophysical study of the Adria plate, *Mem. Soc. Geol. Ital.* **40,** 335–344.

Finetti, I. R., and A. Del Ben (2005). Crustal tectono- stratigraphic setting of the Adriatic Sea from new CROP seismic data, in *CROP Project: Deep Seismic Exploration of the Central Mediterranean and Italy, Atlases in Geoscience*, Vol. 1, I. R. Finetti (Editor), Elsevier, Amsterdam, The Netherlands, 519–547.

Gamage, S., N. Umino, A. Hasegawa, and S. Kirby (2009). Offshore double-planed shallow seismic zone in the NE Japan forearc region revealed by sP depth phases recorded by regional networks, *Geophys. J. Int.* **178,** 195–214, doi: 10.1111/j.1365-246X.2009.04048.x.

Gambini, R., R. Thomas, and S. Morandi (1997). Inversion tectonics on the central Adriatic Sea, *FIST Geoitalia 1997 Abstracts*, Vol. 2, Fed. Ital. di Sci. della Terra, Udine, Italy, 170–171.

Geletti, R., A. Del Ben, M. Busetti, R. Ramella, and V. Volpi (2008). Gas seeps linked to salt structures in the Central Adriatic Sea, *Basin Res.* **20,** no. 4, 473–487, doi: 10.1111/j.1365-2117.2008.00373.x.

Geletti, R., A. Del Ben, M. Busetti, and V. Volpi (2020). Evidenze di gas-seepage associate a strutture tettoniche profonde in Mare Adriatico Centrale, *Mem. Descr. Carta Geol. d'It.* **105,** 25–28 (in Italian).

Giustiniani, M., U. Tinivella, S. Parolai, F. Donda, G. Brancolini, and V. Volpi (2020). Integrated geophysical analyses of shallow-water seismic imaging with Scholte wave inversion: The northern Adriatic Sea case study, *Front. Earth Sci.* **8,** 587898, doi: 10.3389/feart.2020.587898.

Grandić, S., E. Boromisa-Balas, and M. Sustercic (1997). Exploration concept and characteristics of the stratigraphic and structural models of the Dinarides, in Croatian offshore area, Part II: Hydrocarbon consideration, *NAFTA* **48,** nos. 8/9, 249–266.

Grandić, S., I. Kratković, and I. Rusan (2010). Hydrocarbon potential assessment of the slope deposits along the SW Dinarides carbonate platform edge, *NAFTA* **61,** nos. 7/8, 325–338.

Handy, M. R., S. M. Schmid, R. Bousquet, E. Kissling, and D. Bernoulli (2010). Reconciling plate-tectonic reconstructions of Alpine Tethys with the geological–geophysical record of spreading and subduction in the Alps, *Earth Sci. Rev.* **102,** nos. 3/4, 121–158.

Herak, D., M. Herak, E. Prelogović, S. Markušić, and Ž. Markulin (2005). Jabuka island (Central Adriatic Sea) earthquakes of 2003, *Tectonophysics* **398,** nos. 3/4, 167–180, doi: 10.1016/j.tecto.2005.01.007.

Herak, M., D. Herak, and S. Markušić (1996). Revision of the earthquake catalogue and seismicity of Croatia, 1908-1992, *Terra Nova* **8,** 86–94.

Huang, Z., and D. Zhao (2013a). Mechanism of the 2011 Tohoku-Oki earthquake (Mw 9.0) and tsunami: Insight from seismic tomography, *J. Asian Earth Sci.* **70,** 160–168.

Huang, Z., and D. Zhao (2013b). Relocating the 2011 Tohoku-Oki earthquakes (M 6.0–9.0), *Tectonophysics* **586,** 35–45.

ISIDe Working Group (2007). Italian Seismological Instrumental and Parametric Database (ISIDe), *Istituto Nazionale di Geofisica e Vulcanologia (INGV)*, doi: 10.13127/ISIDE.

Ivančić, I., D. Herak, M. Herak, I. Allegretti, T. Fiket, K. Kuk, S. Markušić, S. Prevolnik, I. Sović, I. Dasović, and J. Stipčević (2018). Seismicity of Croatia in the period 2006–2015, *Geofizika* **35,** doi: 10.15233/gfz.2018.35.2.

Ivančić, I., D. Herak, S. Markušić, I. Sović, and M. Herak (2006). Seismicity of Croatia in the period 2002–2005, *Geofizika* **23,** 87–103.

Kastelic, V., and M. M. C. Carafa (2012). Fault slip rates for the active External Dinarides thrust-and-fold belt, *Tectonics* **31**, TC3019, doi: 10.1029/2011TC003022.

Kastelic, V., P. Vannoli, P. Burrato, U. Fracassi, M. M. Tiberti, and G. Valensise (2013). Seismogenic sources in the Adriatic Domain, *Mar. Petrol. Geol.* **42,** 191–213, doi: 10.1016/j.marpetgeo.2012.08.002.

Lahr, J. C. (1999). HYPOELLIPSE: A computer program for determining local earthquake hypocentral parameters, magnitude, and first-motion pattern, *U.S. Geol. Surv. Open-File Rept. 99-23*, version 1.1, available at https://pubs.usgs.gov/of/1999/ofr-99-0023/ (last accessed November 2022).

Le Breton, E., M. R. Handy, G. Molli, and K. Ustaszewski (2017). Post-20 Ma motion of the Adriatic plate: New constraints from surrounding Orogens and implications for crust-mantle decoupling, *Tectonics* **36,** doi: 10.1002/2016TC004443.

Liu, X., D. Zhao, and S. Li (2013a). Seismic imaging of the Southwest Japan arc from the Nankai trough to the Japan Sea, *Phys. Earth Planet In.* **216,** 59–73.

Liu, X., D. Zhao, and S. Li (2013b). Seismic heterogeneity and anisotropy of the southern Kuril arc: Insight into megathrust earthquakes, *Geophys. J. Int.* **194,** 1069–1090.

Magnoni, F., E. Casarotti, D. Komatitsch, R. Di Stefano, M. G. Ciaccio, C. Tape, D. Melini, A. Michelini, A. Piersanti, and J. Tromp (2022). Adjoint tomography of the Italian Lithosphere, *Commun. Earth. Environ.* **3,** 69, doi: 10.1038/s43247-022-00397-7.

Maramai, A., L. Graziani, and B. Brizuela (2019). Euro-Mediterranean Tsunami Catalogue (EMTC), version 2.0, *Istituto Nazionale di Geofisica e Vulcanologia (INGV)*, doi: 10.13127/tsunami/emtc.2.0.

Michele, M., D. Latorre, B. Castello, R. Di Stefano, and L. Chiaraluce (2017). High-resolution seismicity catalog of Italian peninsula in the period 1981-2015, *AGU Fall Meeting Abstracts*, Vol. 2017, S53B–0695.

Paulatto, M., T. Pinat, and F. Romanelli (2007). Tsunami hazard scenarios in the Adriatic Sea domain, *Nat. Hazards Earth Syst. Sci.* **7,** no. 2, 309–325.

Peace, D., D. Brown, E. Zappaterra, R. Spoors, G. Scaife, D. Rowlands, and D. Sewell (2012). The Italian Adriatic Sea: Bringing new life to an established region, *The Leading Edge* **31,** no. 7, 802–809, doi: 10.1190/tle31070802.1.

Pfiffner, O. A. (2014). *Geology of the Alps*, John Wiley and Sons, Hoboken, New Jersey.

Riguzzi, F., A. Tertulliani, and C. Gasparini (1989). Study of the seismic sequence of Porto San Giorgio (Marche)–3 July 1987, *Il Nuovo Cimento C* **12,** 453–466, doi: 10.1007/BF02525078.

Sani, F., G. Vannucci, M. Boccaletti, M. Bonini, G. Corti, and E. Serpelloni (2016). Insights into the fragmentation of the Adria Plate, *J. Geodynam.* **102,** 121–138, doi: 10.1016/j.jog.2016.09.004.

Schmid, S. M., B. Fügenschuh, E. Kissling, and R. Schuster (2004). Tectonic map and overall architecture of the Alpine orogen, *Eclogae Geol. Helv.* **97,** no. 1, 93–117.

Scisciani, V., and F. Calamita (2009). Active intraplate deformation within Adria: Examples from the Adriatic region, *Tectonophysics* **476,** nos. 1/2, 57–72, doi: 10.1016/j.tecto.2008.10.030.

Scrocca, D. (2006). Thrust front segmentation induced by differential slab retreat in the Apennines (Italy), *Terra Nova* **18,** 154–161.

Scrocca, D., E. Carminati, C. Doglioni, and D. Marcantoni (2007). Slab retreat and active shortening along the Central-Northern Apennines, in *Thrust Belt and Foreland Basins, From Fold Kinematics to Hydrocarbon Systems*, O. Lacombe, J. Lavé, F. Roure, and J. Verges, (Editors), Front. Earth Sci., Springer, Berlin, Germany, 471–487.

Selva, J., S. Lorito, M. Volpe, F. Romano, R. Tonini, P. Perfetti, F. Bernardi, M. Taroni, A. Scala, A. Babeyko, *et al.* (2021). Probabilistic tsunami forecasting for early warning, *Nat. Commun.* **12,** 5677, doi: 10.1038/s41467-021-25815-w.

Stampfli, G. M., and G. D. Borel (2002). A plate tectonic model for the paleozoic and mesozoic constrained by dynamic plate boundaries and restored synthetic oceanic Isochrons, *Earth Planet. Sci. Lett.* **196,** 17–33, doi: 10.1016/S0012-821X(01)00588-X.

Stein, S., and D. A. Wiens (1986). Depth determination for shallow teleseismic earthquakes: Methods and results, *Rev. Geophys.* **24,** no. 4, 806–832, doi: 10.1029/RG024i004p00806.

Stoppa, F. (2014). Reminiscences of the great tsunami of July 1627 in the Frentana coast: The case of Lanciano—San Vito Chietino, *Atti Conferenza Nazionale ISPRA*, Policoro (MT), 349–356.

Strollo, A., D. Cambaz, J. Clinton, P. Danecek, C. P. Evangelidis, A. Marmureanu, L. Ottemöller, H. Pedersen, R. Sleeman, K. Stammler, *et al.* (2021). EIDA: The European integrated data archive and service infrastructure within ORFEUS. *Seismol. Res. Lett.* **92,** no. 3, 1788–1795, doi: 10.1785/0220200413.

Tinti, S., A. Maramai, and L. Graziani (2004). The new catalogue of Italian Tsunamis, *Nat. Hazards* **33,** 439–465, doi: 10.1023/B:NHAZ.0000048469.51059.65.

Trincardi, F., A. Cattaneo, A. Asioli, A. Correggiari, and L. Langone (1996). Stratigraphy of the late-Quaternary deposits in the central Adriatic basin and the record of short-term climatic events, *Mem. Istit. Ital. Idrobiol.* **55,** 39–70.

Trincardi, F., A. Cattaneo, A. Correggiari, and D. Ridente (2004). Evidence of soft sediment deformation, fluid escape, sediment failure and regional weak layers within the late Quaternary mud deposits of the Adriatic Sea, *Mar. Geol.* **213,** 91–119, doi: 10.1016/j.margeo.2004.10.003.

Trümpy, R. (1960). Paleotectonic evolution of the Central and Western Alps, *Geol. Soc. Am. Bull.* **71,** no. 6, 843–907.

Umino, N., and A. Hasegawa (1994). Aftershock focal depths of the 1993 Hokkaido-Nansei-Oki earthquake estimated from sP depth phase at small epicentral distances, *J. Phys. Earth* **42,** 4, doi: 10.4294/jpe1952.42.321.

Umino, N., A. Hasegawa, and T. Matsuzawa (1995). sP depth phase at small epicentral distances and estimated subducting plate boundary, *Geophys. J. Int.* **120,** 356–366, doi: 10.1111/j.1365-246X.1995.tb01824.x.

Van Straaten, L. M. J. V. (1970). Holocene and late-Pleistocene sedimentation in the Adriatic Sea, *Geol. Rundschau* **60,** 106–131.

Vrdoljak, L., M. Režic, and I. Petricevic (2021). Bathymetric and geological properties of the Adriatic Sea, *Rudarsko-Geolosko-Naftni Zbornik* **36,** no. 2, 93–107, doi: 10.17794/rgn.2021.2.9.

Wessel, P., J. F. Luis, L. Uieda, R. Scharroo, F. Wobbe, W. H. F. Smith, and D. Tian (2019). The generic mapping tools version 6, *Geochem. Geophys. Geosys.* **20,** 5556–5564, doi: 10.1029/2019GC008515.

Zhao, D. (2019). Importance of later phases in seismic tomography, *Phys. Earth Planet. In.* **296,** 106314, doi: 10.1016/j.pepi.2019.106314.

Zhao, D., Z. Huang, N. Umino, A. Hasegawa, and T. Yoshida (2011). Seismic imaging of the Amur-Okhotsk plate boundary zone in the Japan Sea, *Phys. Earth Planet. In.* **188,** 82–95.

Zhao, D., O. P. Mishra, and R. Sanda (2002). Influence of fluids and magma on earthquakes: Seismological evidence, *Phys. Earth Planet. In.* **132,** 249–267.

Zhao, D., Z. Wang, N. Umino, and A. Hasegawa (2007). Tomographic imaging outside a seismic network: Application to the northeast Japan arc, *Bull. Seismol. Soc. Am.* **97,** 1121–1132.

**Manuscript received 17 June 2022**
**Published online 2 December 2022**